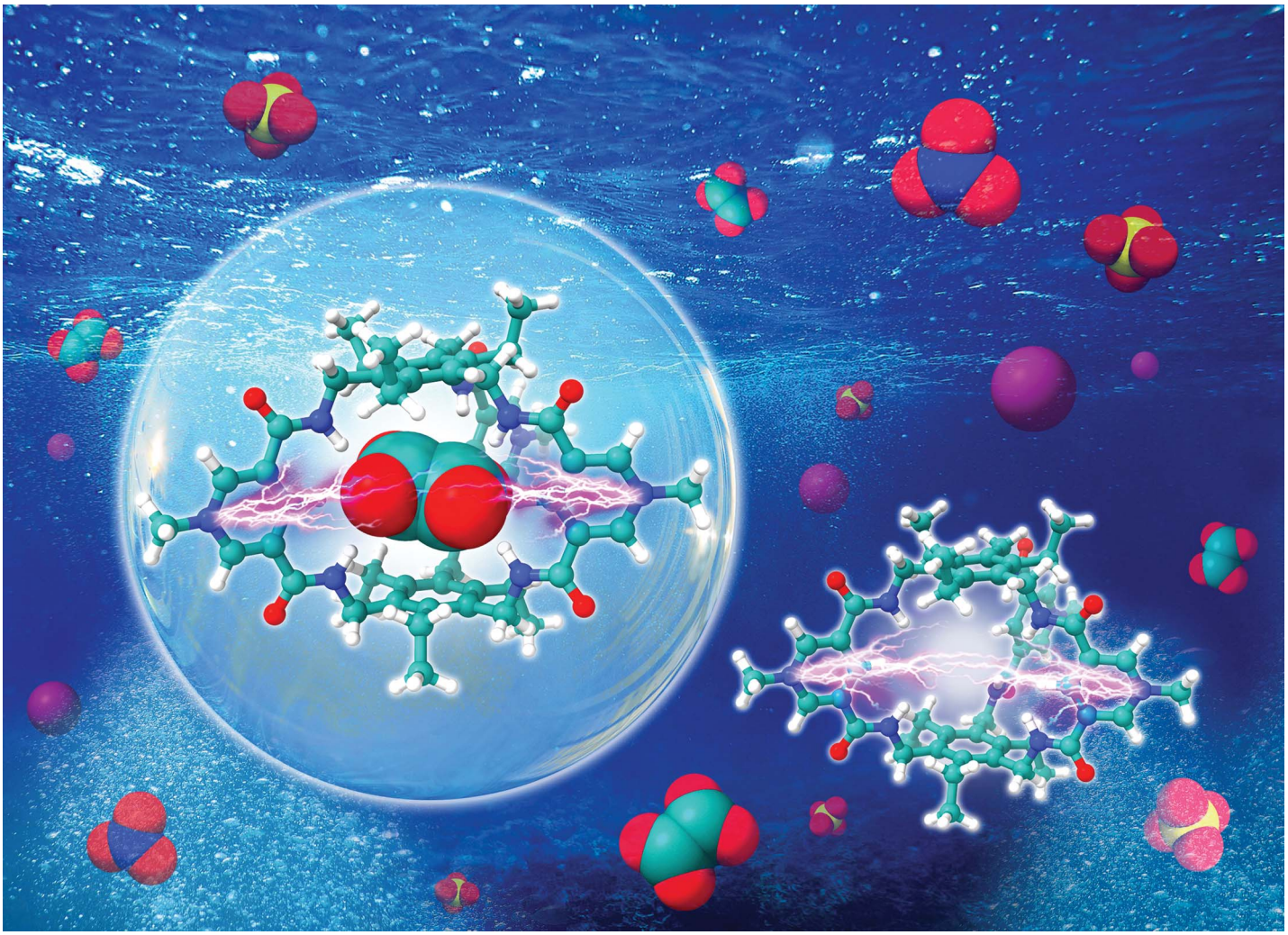

Showcasing research from Professor Wenqi "Vince" Liu laboratory, Department of Chemistry, University of South Florida, Tampa, United States.

Charge-assisted hydrogen bonding in a bicyclic amide cage: an effective approach to anion recognition and catalysis in water

We present a water-soluble hydrogen bonding cage with remarkable affinity and selectivity for highly hydrophilic anions such as sulfate and oxalate. Our molecular design strategy, utilizing charge-assisted hydrogen bonding in amide-based receptors, revalidates the critical role of hydrogen bonding for anion recognition in water. Additionally, we reveal a novel catalytic mechanism in which the cationic cage encapsulates anionic oxalate, reversing its charge and overcoming electrostatic repulsion to facilitate oxidation by permanganate.

As featured in:

See Wenqi Liu *et al.*, *Chem. Sci.*, 2024, **15**, 16040.

ROYAL SOCIETY OF CHEMISTRY

rsc.li/chemical-science

Registered charity number: 207890

Chemical Science

ROYAL SOCIETY OF CHEMISTRY

EDGE ARTICLE

View Article Online
View Journal | View Issue

Cite this: *Chem. Sci.*, 2024, **15**, 16040

All publication charges for this article have been paid for by the Royal Society of Chemistry

Received 5th August 2024
Accepted 9th September 2024

DOI: 10.1039/d4sc05236f

rsc.li/chemical-science

Charge-assisted hydrogen bonding in a bicyclic amide cage: an effective approach to anion recognition and catalysis in water†

Chengkai Xu, Quy Gia Tran, Dexin Liu, Canjia Zhai, Lukasz Wojtas and Wenqi Liu *

Hydrogen bonding is prevalent in biological systems, dictating a myriad of life-sustaining functions in aqueous environments. Leveraging hydrogen bonding for molecular recognition in water encounters significant challenges in synthetic receptors on account of the hydration of their functional groups. Herein, we introduce a water-soluble hydrogen bonding cage, synthesized *via* a dynamic approach, exhibiting remarkable affinities and selectivities for strongly hydrated anions, including sulfate and oxalate, in water. We illustrate the use of charge-assisted hydrogen bonding in amide-type synthetic receptors, offering a general molecular design principle that applies to a wide range of amide receptors for molecular recognition in water. This strategy not only revalidates the functions of hydrogen bonding but also facilitates the effective recognition of hydrophilic anions in water. We further demonstrate an unconventional catalytic mechanism through the encapsulation of the anionic oxalate substrate by the cationic cage, which effectively inverts the charges associated with the substrate and overcomes electrostatic repulsions to facilitate its oxidation by the anionic MnO_4^-. Technical applications using this receptor are envisioned across various technical applications, including anion sensing, separation, catalysis, medical interventions, and molecular nanotechnology.

Introduction

Hydrogen bonding plays a crucial role in nature, enabling biological receptors to recognize hydrated substrates. This mechanism underpins numerous vital functions in aqueous environments.[1–5] However, replicating this process with synthetic analogs poses significant challenges, particularly in using hydrogen bonds for substrate recognition in water.[6–9] One major hurdle is the strong hydration of both receptor and substrate, creating high energetic barriers due to the need for desolvation during the binding process. Additionally, most organic building blocks used to synthesize hydrogen bonding receptors are poorly soluble in water, complicating the design and synthesis of water-soluble receptors. The pursuit of water-soluble hydrogen bonding receptors capable of effectively recognizing strongly hydrated substrates marks a cutting-edge frontier in supramolecular chemistry. Achieving this functionality could have profound impacts across various fields, including catalytic chemical transformations, biology, healthcare, environmental science, and molecular nanotechnology.[10–16]

Current approaches to revalidating hydrogen bonding in water mainly focus on two strategies: hydrophobicity-assisted and charge-assisted hydrogen bonding. Hydrophobicity-assisted hydrogen bonding, in particular, involves the design of receptors that mimic the structure of protein-binding pockets.[17–20] These receptors feature hydrogen bonding residues buried within a hydrophobic binding pocket. This design leverages the hydrophobic effect to offset the energy cost of dehydration, thus serving as the primary driving force. At the same time, hydrogen bonding ensures the selectivity in the binding process. This approach has successfully been applied in a variety of hydrogen bonding receptors, such as molecular temples,[21–27] tetralactam macrocycles,[19,20,28–31] naphthotubes,[32–40] and cyclopeptides,[41–43] demonstrating its viability and effectiveness.

Charge-assisted hydrogen bonding is another critical strategy for the binding of anionic substrates in water, leveraging electrostatic interactions to offset hydration energy. However, this strategy is predominantly confined to polyammonium and guanidinium receptors. Polyammonium receptors exhibit[44,45] (Fig. 1a, left) high effectiveness in acidic conditions but lose their anion-binding efficiency and water solubility under neutral or basic pH, thereby restricting their applications. Guanidinium-based receptors can maintain[8,9,46–48]

Department of Chemistry, University of South Florida, 4202 E. Fowler Ave, Tampa, FL, 33620, USA. E-mail: wenqi@usf.edu

† Electronic supplementary information (ESI) available. CCDC 2334098 and 2334101–2334103. For ESI and crystallographic data in CIF or other electronic format see DOI: https://doi.org/10.1039/d4sc05236f

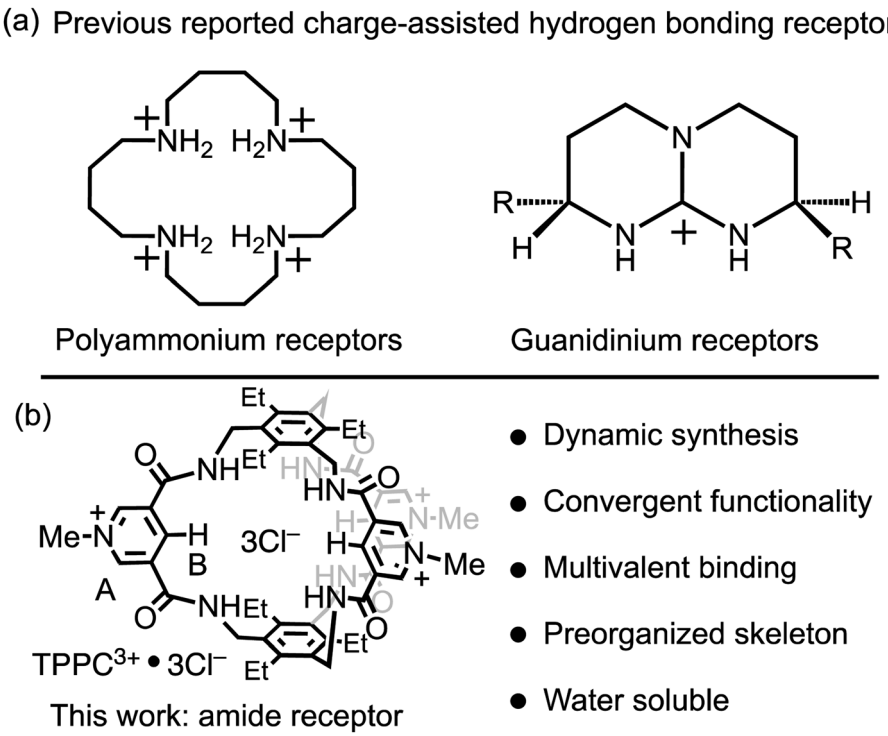

Fig. 1 (a) Representative anion receptors with charge-assisted hydrogen bonding functionalities. (b) The structural formula of $TPPC^{3+}\cdot 3Cl^{-}$ and a summary of its structural features.

(Fig. 1a, right) their charge in neutral environments but face challenges in conformational flexibility and strong solvation. For instance, a single guanidinium ion's binding with carbonate or phosphate in water is negligible, with a binding constant (K_a) of less than 5 M^{-1}.[9] This limitation narrows the charge-assisted hydrogen bonding application in guanidinium receptors to specific molecular frameworks that either incorporate constrained amino imidazoline, bicyclic guanidinium residues, or use multiple guanidinium groups for anion binding.[11,46–50] This restriction significantly limits the diversity of molecular scaffolds available for receptor design. Consequently, despite the effectiveness of leveraging electrostatic interactions in enhancing hydrogen bonds in water, there is a pressing need for a broader molecular design strategy to fully exploit the power of charge-assisted hydrogen bonding.

Hydrogen-bonding receptors, especially those utilizing amide functionalities, have been the subject of extensive research in the field of anion recognition. However, the majority of this research has focused[51–67] on anion binding in organic solvents. Given the significant number of hydrogen bonding receptors that either cannot bind anions in water due to solubility issues or lose their effectiveness because of strong solvation, there is a crucial need for a universal molecular design strategy that revalidates the hydrogen bonding capability of these receptors through the principle of charge-assisted hydrogen bonding. Such a strategy promises to have a far-reaching impact on the field of anion recognition in water.

In this research, we showcase a general approach to revalidate the hydrogen bonding capability of amide receptors for anion recognition in water. We demonstrate a water-soluble tripodal tricationic cage-type receptor $TPPC^{3+}\cdot 3Cl^{-}$ under the principle of charge-assisted hydrogen bonding. The receptor utilizes (Fig. 1b) pyridinium moieties both as charge carriers and for water solubilization groups.[68–71] The introduction of positive charges creates electrostatic attractions with anions, which serve as the driving force to overcome their dehydration energy barrier, while hydrogen bonding patterns within the binding pocket provide substrate selectivity. This receptor is synthesized through a dynamic process, beginning with an imine condensation reaction, followed by a crucial imine-to-amide oxidation step to complete the cyclization. $TPPC^{3+}\cdot 3Cl^{-}$ exhibits remarkable affinities and selectivities for hydrophilic anions such as $C_2O_4^{2-}$, SO_4^{2-}, and NO_3^{-}. The binding to these hydrophilic anions is primarily driven by a favorable entropic effect resulting from the anion desolvation upon their associations by the cage. Additionally, the encapsulation of $HC_2O_4^{-}$ by $TPPC^{3+}$ inverts its overall charge, forming the $[HC_2O_4^{-}\subset \star TPPC^{3+}]^{2+}$ complex. This charge inversion overcomes the electrostatic repulsion and increases the reactivity between $HC_2O_4^{-}$ and MnO_4^{-}. As a result, $TPPC^{3+}\cdot 3Cl^{-}$ shows a catalyst activity for the oxidation of $HC_2O_4^{-}$ by MnO_4^{-}, illustrating its practical application in catalytic chemical transformation in water.

Results and discussion

Molecular design and synthesis

The 3,5-dicarboxamide pyridinium building block has been extensively explored by the Beer group in mechanically

interlocked structures, leveraging the charge and hydrogen bonds for anion recognition in organic solvents.[72–79] As a proof of principle for charge-assisted hydrogen bonding in amide-based receptors, we have introduced (Fig. 1b) this pyridinium moiety as the charge carrier into a rigid, preorganized bicyclic molecular cage developed by Anslyn and Mastalerz.[59,80–82] The trimethyl pinwheel-shaped pyridinium cage, $TPPC^{3+}\cdot 3Cl^{-}$, is equipped with six hydrogen bond donors converging towards its binding cavity. The C–H bonds at the *para* position of the pyridinium rings are polarized, creating three additional hydrogen bond donors pointing toward the cavity.[69,71] Additionally, the three pyridinium residues serve as charge carriers, assisting the hydrogen bonding by providing electrostatic attractions with anions in water. When associated with the hydrophilic counter-anion Cl^{-}, the receptor maintains good water solubility.[83] This molecular design strategy exemplifies a general approach that could be extended to other amide-based hydrogen bonding receptors for binding hydrophilic substrates in water.[54,55]

The $TPPC^{3+}\cdot 3Cl^{-}$ cage can be synthesized (Fig. 2) through two distinct methods. The first method involves a traditional approach, where acyl chloride 2 is reacted with the pinwheel-shaped triamine 1 under high dilution conditions. This process results in the critical intermediate, amide cage 5, at a low yield of 9%, which is common for irreversible macrocyclization reactions not relying on the use of a template.[84–88] An alternative and more effective method employs[68,81,82,89] dynamic imine chemistry followed by the Pinnick oxidation reaction. The triamine 1 is condensed with bisaldehyde 3, leading to a quantitative formation of the bicyclic imine skeleton. The resulting imine cage 4 can then be converted into the key intermediate amide cage 5 through Pinnick oxidation, achieving a much higher yield of 61%. The final steps involve alkylating the pyridine moiety to form a pyridinium salt, followed by standard anion exchange with a yield of 76%. These three steps produce the water-soluble amide cage $TPPC^{3+}\cdot 3Cl^{-}$ with an overall yield of 46% from easily accessible starting materials.

Anions binding in water

The anion-binding properties of $TPPC^{3+}\cdot 3Cl^{-}$ in water were analyzed through ^{1}H NMR titration experiments. Our findings (Fig. S45†) show that the chemical shift of the inward-facing C–H proton B depends on the concentration of $TPPC^{3+}\cdot 3Cl^{-}$, indicating that the cage is partially occupied by Cl^{-} counter anions and exists as a mixture of $TPPC^{3+}$ and $Cl^{-}\subset TPPC^{3+}$. Therefore, the anion binding affinities measured should be considered as apparent binding affinities, reflecting the displacement of chloride ions from the binding cavity by the target anions. To avoid D/H exchange between the protons from the cage and D_2O and to obtain direct evidence of the hydrogen bonding between the anions and $TPPC^{3+}\cdot 3Cl^{-}$, we performed the experiments in a solution of 10% D_2O and 90% H_2O. The broad peak around 8.84 pm represents the NH proton signals. Upon the addition of Na_2SO_4, this peak showed dramatic downfield shifts ($\Delta\delta$ = +0.69 ppm), suggesting the hydrogen bonds formation between SO_4^{2-} and the NH protons from $TPPC^{3+}\cdot 3Cl^{-}$ in water. The inward-facing C–H protons, labeled (Fig. 1b) as proton B, are polarized, making them effective hydrogen bond donors. The binding of SO_4^{2-} by $TPPC^{3+}\cdot 3Cl^{-}$ results (Fig. 3a) in a notable upfield shift ($\Delta\delta = -0.15$ ppm) of proton B. This observed shift in proton B indicates a change in the hydrogen bonding state of these protons, likely transitioning from bonding with H_2O or Cl^{-} to SO_4^{2-}. Nonlinear fitting of the chemical shift changes of proton B against the concentration of SO_4^{2-}, based on a 1 : 1 binding model, yielded an apparent binding constant (K_a) of $(1.7 \pm 0.1) \times 10^4\ M^{-1}$. In a separate experiment, where the titration was performed in D_2O, the same trend in the changes of the chemical shifts was

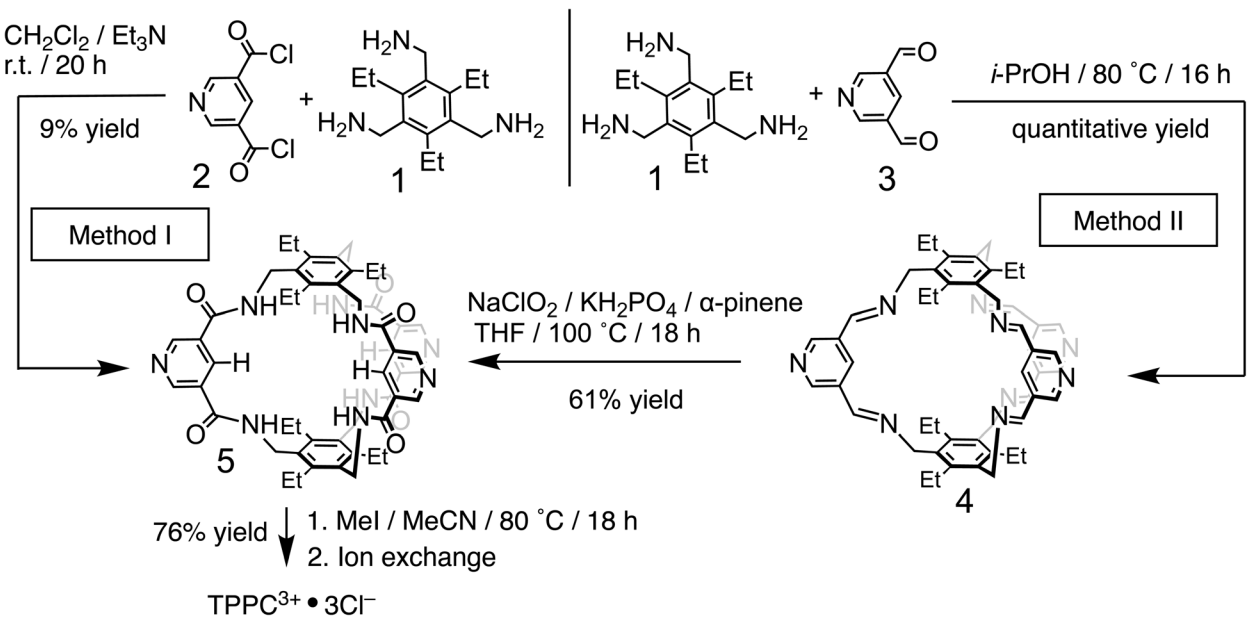

Fig. 2 Synthesis of $TPPC^{3+}\cdot 3Cl^{-}$ using a conventional high dilution approach (method I) and a dynamic approach (method II).

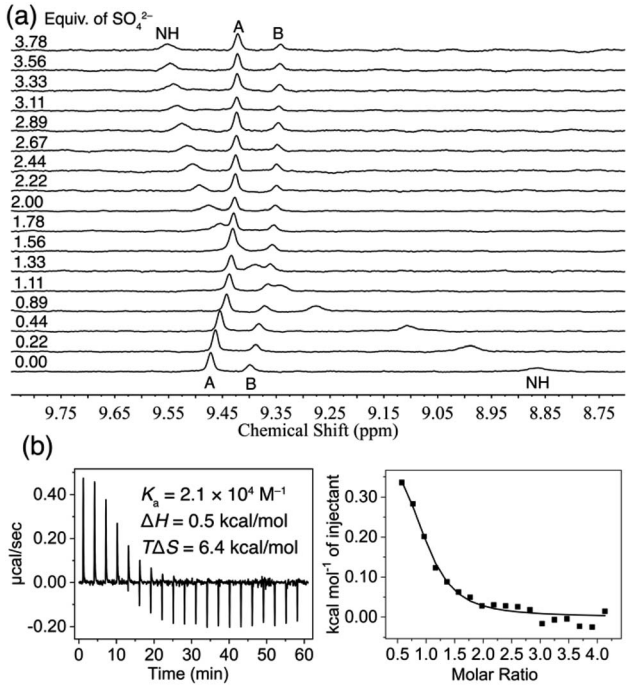

Fig. 3 (a) ^{1}H NMR spectra (400 MHz, 10% D_2O + 90% H_2O) of $TPPC^{3+}\cdot 3Cl^-$ (0.1 mM) titrated with Na_2SO_4. (b) ITC profile of $TPPC^{3+}\cdot 3Cl^-$ (0.5 mM) titrated with Na_2SO_4 in H_2O.

observed (Fig. S37†). The nonlinear fitting of the changes in the chemical shift of proton B in D_2O yielded (Fig. S38†) a similar apparent binding affinity of $(2.5 \pm 0.3) \times 10^4$ M^{-1}.

The binding of SO_4^{2-} by $TPPC^{3+}\cdot 3Cl^-$ was further confirmed using isothermal titration calorimetry (ITC). A solution of Na_2SO_4 in H_2O was incrementally added to a 0.5 mM solution of $TPPC^{3+}\cdot 3Cl^-$, and the heat change in the system was monitored over time. The ITC data revealed (Fig. 3b) an endothermic binding process mainly assigned to the interaction between SO_4^{2-} and $TPPC^{3+}$. Analyzing the binding isotherm with a 1 : 1 binding model yielded an apparent binding affinity similar to our previous findings at a K_a of $(2.0 \pm 0.6) \times 10^4$ M^{-1}. The ITC results indicated that the binding is primarily driven by favorable entropy ($-T\Delta S = -6.35$ kcal mol^{-1}), with only a minor enthalpic penalty ($\Delta H = +0.48$ kcal mol^{-1}). This outcome aligns with our hypothesis that the dehydration of the highly hydrophilic SO_4^{2-} demands significant enthalpic energy. The combined hydrogen bonding and electrostatic interactions between SO_4^{2-} and $TPPC^{3+}\cdot 3Cl^-$ do not completely offset this high enthalpic requirement, resulting in a small net enthalpic penalty of +0.48 kcal mol^{-1}. At the same time, the dehydration process releases water molecules from both the hydration shell of SO_4^{2-} and the binding cavity of the cage into the bulk solution, providing a substantial entropic driving force for the molecular recognition of this hydrophilic anion. Such an entropically driven binding mechanism, commonly observed in the association of hydrophobic molecules in water (known as the hydrophobic effect), is rare for hydrophilic substrates as it typically requires significant enthalpic compensation for dehydration.[8,90] In this case, charge-assisted hydrogen bonding proves to be a unique and effective strategy to facilitate the dehydration of hydrophilic anions in water.

The binding pattern of $C_2O_4^{2-}$ anion with $TPPC^{3+}\cdot 3Cl^-$ presents distinct characteristics compared to that of SO_4^{2-}. The ^{1}H NMR spectra of $TPPC^{3+}\cdot 3Cl^-$ obtained in a mixture of 10% D_2O and 90% H_2O show (Fig. 4a) notable downfield shifts for both the NH protons ($\Delta\delta$ = + 0.65 ppm) and protons B ($\Delta\delta$ = +0.35 ppm) with an increasing concentration of $Na_2C_2O_4$. This result serves as direct evidence of hydrogen bonding formation between $TPPC^{3+}$ and $C_2O_4^{2-}$ in water. Nonlinear fitting of changes in the chemical shift of proton B yielded a K_a higher than 10^6 M^{-1}. This strong apparent binding affinity was independently corroborated by ITC, which indicated (Fig. 4b) a K_a of $(2.0 \pm 0.9) \times 10^6$ M^{-1}. The ITC experiments revealed an exothermic process for this binding, with a favorable enthalpic contribution (ΔH) of -3.3 kcal mol^{-1}. Additionally, a substantial favorable entropic contribution ($-T\Delta S = -5.3$ kcal mol^{-1}) was identified as the primary driving force for the interaction between $C_2O_4^{2-}$ and $TPPC^{3+}$. These results suggest that the charge-assisted hydrogen bond not only overcomes the dehydration barrier of $C_2O_4^{2-}$ but also provides additional binding enthalpy, serving as an additional driving force for the recognition of hydrophilic $C_2O_4^{2-}$ anion in water. More importantly, the anion binding facilitated by charge-assisted hydrogen bonding significantly benefits from the release of constrained water molecules from both the hydration shell of the anions and the binding pocket of the cage. This entropic effect serves as the primary driving force behind the effective anion binding in water.

The binding affinities of $TPPC^{3+}\cdot 3Cl^-$ with various anions in water are detailed in Table 1. $TPPC^{3+}$ shows a strong affinity for

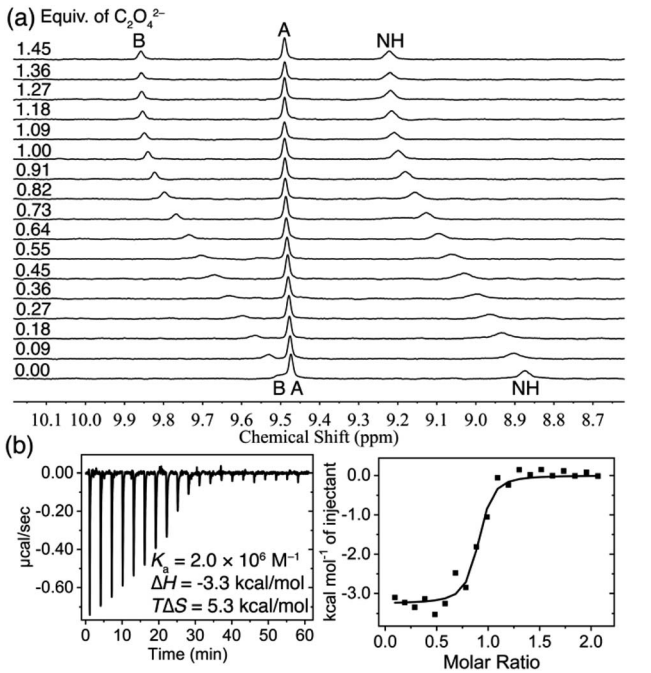

Fig. 4 (a) ^{1}H NMR spectra (400 MHz, 10% D_2O + 90% H_2O) of $TPPC^{3+}\cdot 3Cl^-$ (0.2 mM) titrated with $Na_2C_2O_4$. (b) ITC profile of $TPPC^{3+}\cdot 3Cl^-$ (0.1 mM) titrated with $Na_2C_2O_4$ in H_2O.

I^- and NO_3^-, with similar binding strengths in the order of 10^4 M^{-1}. AcO^- and NO_2^- exhibit comparable affinities, each around 1500 M^{-1}, while Br^- and Cl^- are both around 600 M^{-1}. In terms of selectivity for halide anions,[91] we observed a trend of $I^- > Br^- \approx Cl^-$. The higher affinity for I^- compared to Br^- and Cl^- suggests that the hydrophobic effect is a predominant driving force in anion binding in water. Although Br^- is more hydrophobic than Cl^-, Br^- has a lower charge density, resulting in similar apparent binding affinities for both anions. This observation indicates that electrostatic interactions may also play a significant role in binding. Generally, $TPPC^{3+}$ demonstrates higher affinities for anions with more negative charges, as evident in the observed trend: $C_2O_4^{2-} > SO_4^{2-} > NO_3^-$. Additionally, $TPPC^{3+}$ shows notable shape selectivity in anion binding. More binding sites correlate with higher affinity, and anions with similar structures exhibit comparable affinities, as seen in the trend $NO_3^- > AcO^- \approx NO_2^-$. Further thermodynamic analysis indicates that the anion binding by $TPPC^{3+}$ is consistently associated with a positive entropy change, which acts as a major driving force in the recognition process. Overall, $TPPC^{3+}\cdot 3Cl^-$ demonstrates effective selectivity in anion binding in water. This selectivity is influenced by a combination of factors, including electrostatic attraction, shape complementarity, and hydrophobicity.

Structural analysis by X-ray single crystallography and DFT calculations

Three distinct single crystal structures of $TPPC^{3+}$ were obtained (Fig. 5a–c), corresponding to its association with Cl^-, I^-, and $CF_3CO_2^-$ as counter anions. In all these structures, $TPPC^{3+}$ maintains a similar conformation, with all NH bonds converging toward the binding cavity. In the Cl^- complex (Fig. 5a), two Cl^- anions and one water molecule were found within the $TPPC^{3+}$ binding pocket. Each Cl^- forms two [NH···O] and one [CH···O] hydrogen bonds with one of the three pyridinium panels. Additionally, a water molecule located in the cavity aligns its hydrogens toward the two Cl^- guests, forming [OH···Cl] hydrogen bonds. The I^- complex (Fig. 5b) is analogous to the Cl^- complex, with each $TPPC^{3+}$ binding two I^- ions and one water molecule through hydrogen bonds in its binding pocket. In the case of the $CF_3CO_2^-$ complex (Fig. 5c), three $CF_3CO_2^-$ anions are associated with each $TPPC^{3+}$. Each carboxylate group interacts with two of the three pyridinium units, with each oxygen in the carboxylate group forming one [NH···O] and one [CH···O] hydrogen bond with the pyridinium unit.

Table 1 Summary of anions binding in water by $TPPC^{3+}\cdot 3Cl^-$

Anions[a]	K_a/M^{-1} (NMR)[b]	K_a/M^{-1} (ITC)[c]	ΔH/kcal mol^{-1}	$T\Delta S$/kcal mol^{-1}
$C_2O_4^{2-}$	>10^6[d]	$(2.0 \pm 0.9) \times 10^6$	−3.3	5.3
SO_4^{2-}	$(2.5 \pm 0.3) \times 10^4$	$(2.0 \pm 0.6) \times 10^4$	0.5	6.4
I^-	$(1.6 \pm 0.2) \times 10^4$	$(0.9 \pm 0.1) \times 10^4$	−1.4	4.0
NO_3^-	$(1.4 \pm 0.1) \times 10^4$	$(1.1 \pm 0.4) \times 10^4$	−1.6	3.9
AcO^-	1614 ± 11	N.A.[e]	N.A.[e]	N.A.[e]
NO_2^-	1439 ± 33	N.A.[e]	N.A.[e]	N.A.[e]
Br^-	643 ± 38	N.A.[e]	N.A.[e]	N.A.[e]
Cl^-	589 ± 25	N.A.[e]	N.A.[e]	N.A.[e]

[a] All anions come with sodium as the counter cation. [b] The titration experiments were performed in D_2O. [c] The titration experiments were performed in H_2O. [d] Apparent binding affinity is too high to be accurately determined by direct ^1H NMR titration. [e] Apparent binding affinity is too low to be accurately determined by ITC.

Notably, the solid-state single-crystal structures were obtained from organic solvents and do not fully represent the binding states observed in water. One key difference lies in the binding stoichiometry. For example, a 2 : 1 binding stoichiometry is observed for binding I^- in the solid state. In contrast, a 1 : 1 binding stoichiometry between I^- and $TPPC^{3+}$ was determined in solution using ^1H NMR titration, where the shift of the inward-facing C–H proton B stopped after adding 1.0 equivalent of I^-. Complementary results supporting the 1 : 1 binding stoichiometry are also found in high-resolution mass spectrometry (HRMS), where the m/z peaks for the 1 : 1 complexes were observed as the major peaks for all anions investigated, indicating that the 1 : 1 complex is the primary species in solution. The absence of m/z peaks for 2 : 1 complexes suggests these species are much less stable and should exist minimally compared to the 1 : 1 complex. In water, anions primarily form 1 : 1 complexes with $TPPC^{3+}$. Forming higher-order anion complexes would require dehydrating a second anion with weaker electrostatic interactions and overcoming strong electrostatic repulsion, making such binding unlikely. In contrast, $TPPC^{3+}$ tends to bind multiple anions in solid-state structures to balance its charges within the crystal lattice. Despite this difference, these crystal structures are valuable as they reveal the conformation of $TPPC^{3+}$ with its convergent functionalities and demonstrate its interactions with anions through hydrogen bonds.

To visualize the potential binding modes of $TPPC^{3+}$ with anions in solution, we carried out structural optimization by DFT calculations at the BLYP-D3/SVP level in implicit water solvent for complexes with Cl^-, Br^-, I^-, NO_3^-, SO_4^{2-}, and $C_2O_4^{2-}$. All halide anions form (Fig. 6a–c and S72–S74†) hydrogen bonds with two of the three pyridinium units, establishing four [NH···O] and two [CH···O] hydrogen bonds. The NO_3^- anion associates (Fig. 6d and S76†) with two pyridinium units of $TPPC^{3+}$ through two [NH···O] and two [CH···O] hydrogen bonds. The SO_4^{2-} anion can interact (Fig. 6e and S77†) with all three pyridinium units of $TPPC^{3+}$. Of its four oxygen atoms of the SO_4^{2-} anion, three of them engage in a total of three [NH···O] and three [CH···O] hydrogen bonds, while the fourth oxygen forms one additional [NH···O] bond. This binding pattern results in a total of seven hydrogen bonds stabilizing the $SO_4^{2-}\subset TPPC^{3+}$ complex. The distances between the oxygen atoms on SO_4^{2-} and the pyridinium nitrogens on $TPPC^{3+}$ range from 5.4 to 6.0 Å, indicating strong electrostatic interactions that stabilize the complex. The larger $C_2O_4^{2-}$ anion fits (Fig. 6f and S78†) better within the $TPPC^{3+}$ cavity. Two of its oxygen atoms form three [NH···O] and three [CH···O] hydrogen bonds with two of the pyridinium units, while the remaining two oxygens form one [NH···O] and two [CH···O] hydrogen bonds with the third unit. This binding pattern results in a total

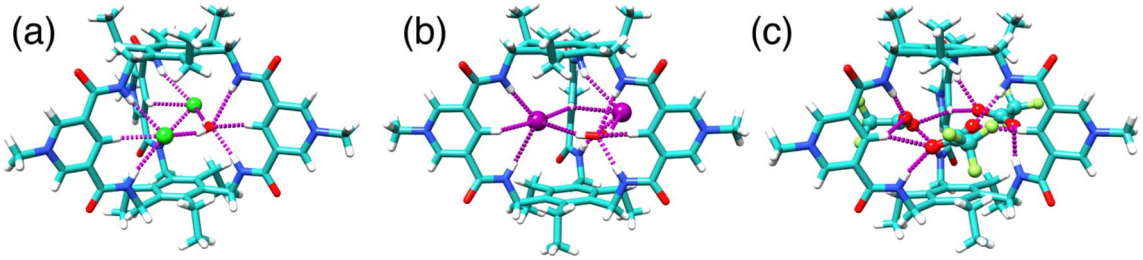

Fig. 5 X-ray single crystal structures of (a) $2Cl^{-}\cdot H_2O\subset TPPC^{3+}$, (b) $2I^{-}\cdot H_2O\subset TPPC^{3+}$, (c) $3CF_3CO_2^{-}\subset TPPC^{3+}$.

of nine hydrogen bonds, stabilizing the $C_2O_4^{2-}\subset TPPC^{3+}$ complex. The distances between the oxygen atoms on $C_2O_4^{2-}$ and the pyridinium nitrogens on $TPPC^{3+}$ are measured at 5.8 to 5.9 Å, suggesting strong electrostatic interactions that stabilize the $C_2O_4^{2-}\subset TPPC^{3+}$ complex.

Catalysis for oxalate oxidation

We next explored how oxalate encapsulation in water with $TPPC^{3+}\cdot 3Cl^{-}$ affects its reactivity in the oxidation process by the permanganate anion. This reaction between permanganate and oxalate is a well-known example of redox reactions exhibiting autocatalytic kinetics.[92–96] The reaction involves (Fig. 7a) $C_2O_4^{2-}$ or $HC_2O_4^{-}$ (depending on the pH) and MnO_4^{-}, yielding Mn^{2+} and CO_2. Initially, the electrostatic repulsion between $HC_2O_4^{-}$ and MnO_4^{-} results in a sluggish reaction rate. The reaction product, Mn^{2+}, acts as a catalyst by forming a neutral complex with $C_2O_4^{2-}$ as MnC_2O_4, which can be more efficiently oxidized by MnO_4^{-} to produce CO_2 and more Mn^{2+}. This newly formed Mn^{2+} further catalyzes the reaction, leading to a characteristic reaction kinetics with an initial induction period needed to generate sufficient Mn^{2+} catalyst, followed by a rapid reaction rate acceleration.[94] We hypothesize (Fig. 7b) that $TPPC^{3+}\cdot 3Cl^{-}$ can act as a catalyst to bypass the initial electrostatic repulsion between $HC_2O_4^{-}$ and MnO_4^{-}, thereby speeding up the reaction by eliminating the induction period.

To test our hypothesis, we mixed a solution of $KMnO_4$ (0.2 mM) with $H_2C_2O_4$ (1 mM) and monitored (Fig. 7c) the reaction by observing the decrease in the $KMnO_4$ absorbance band at 400–700 nm. Initially, the reaction progressed slowly, with only 20% of the $KMnO_4$ reduced (Fig. 7e) by $H_2C_2O_4$ in the first 60 minutes, marking the induction period. From 60 to 95 minutes, the reaction rate significantly increased, resulting in an 80% overall reduction of $KMnO_4$. Introducing 5% $TPPC^{3+}\cdot 3Cl^{-}$ (0.01 mM) into the $KMnO_4$ and $H_2C_2O_4$ mixture drastically accelerated (Fig. 7d) the reaction, with the $KMnO_4$ absorbance band dropping (Fig. 7e) to zero within 30 minutes, indicating a remarkable catalytic effect of $TPPC^{3+}\cdot 3Cl^{-}$. Monitoring the absorbance at 525 nm over time showed the absence of an induction period with the addition of 5% $TPPC^{3+}\cdot 3Cl^{-}$. The catalysis of oxalate oxidation by $KMnO_4$ with $TPPC^{3+}\cdot 3Cl^{-}$ is efficient even at a catalyst load (Fig. 7e) as low as 1%, attributed to the strong affinity between $HC_2O_4^{-}$ and $TPPC^{3+}$ in water.[97] With 10% $TPPC^{3+}\cdot 3Cl^{-}$ as the catalyst, the reaction achieved an 80% MnO_4^{-} reduction in just 20 minutes, which is 4.8 times faster than the autocatalytic reaction without $TPPC^{3+}\cdot 3Cl^{-}$ as the catalyst. The catalytic turnover number was estimated at 70 when 1% of the $TPPC^{3+}$ was used as the catalyst.

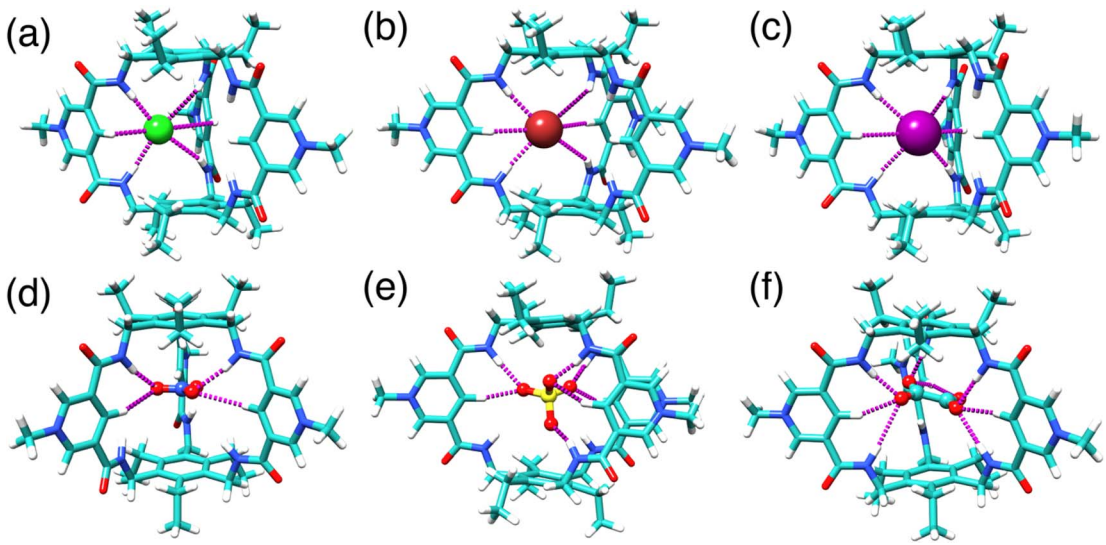

Fig. 6 DFT optimized structure of (a) $Cl^{-}\subset TPPC^{3+}$, (b) $Br^{-}\subset TPPC^{3+}$, (c) $I^{-}\subset TPPC^{3+}$, (d) $NO_3^{-}\subset TPPC^{3+}$, (e) $SO_4^{2-}\subset TPPC^{3+}$, and (f) $C_2O_4^{2-}\subset TPPC^{3+}$.

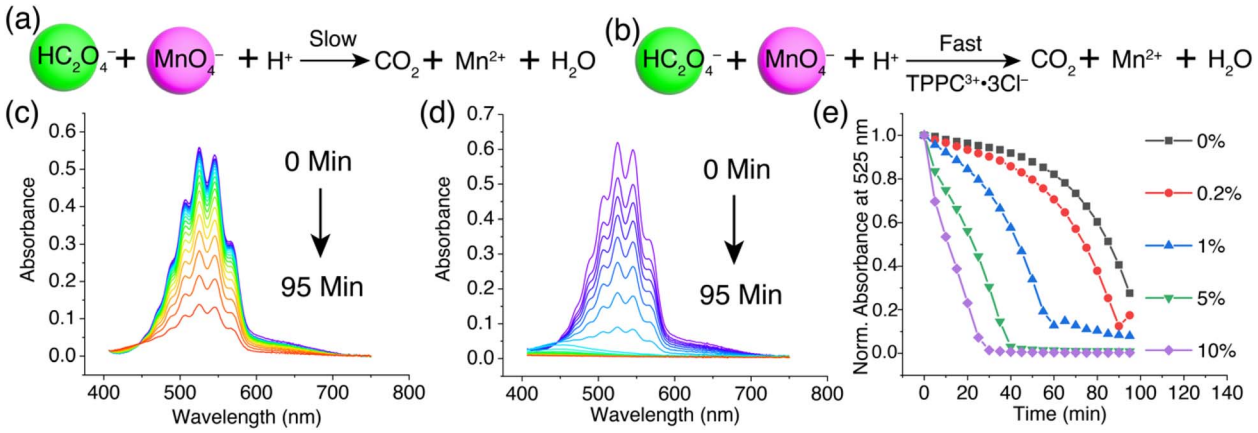

Fig. 7 Reaction formula showing (a) the slow oxidation of oxalate by MnO_4^- and (b) its rate acceleration by $TPPC^{3+}\cdot 3Cl^-$. (c) Changes of the UV-vis spectra in a $KMnO_4$ solution (0.2 mM) over 95 minutes after adding $H_2C_2O_4$ (1 mM). (d) Changes of the UV-vis spectra in a $KMnO_4$ (0.2 mM) solution in the presence of 5% $TPPC^{3+}\cdot 3Cl^-$ (0.01 mM) over 95 minutes following $H_2C_2O_4$ addition (1 mM). (e) The changes in absorbance at 525 nm for a $KMnO_4$ solution (0.2 mM) over 95 minutes, demonstrating the effects of different loadings of $TPPC^{3+}\cdot 3Cl^-$ as a catalyst on the reaction rate post $H_2C_2O_4$ (1 mM) addition.

The catalytic mechanism facilitated by $TPPC^{3+}\cdot 3Cl^-$ is illustrated in Fig. 8 and is relatively straightforward. The encapsulation of $HC_2O_4^-$ by $TPPC^{3+}$ forms a complex ($HC_2O_4^-\subset TPPC^{3+}$) carrying a net charge of +2. This electrostatic attraction between the encapsulated complex and MnO_4^- enhances the oxidation of $HC_2O_4^-$ into CO_2, subsequently releasing the free $TPPC^{3+}$ cage to capture another $HC_2O_4^-$ molecule, thereby perpetuating the catalytic cycle. To validate the effect of molecular recognition between $TPPC^{3+}$ and $HC_2O_4^-$ on the observed catalytic effect, we synthesized (Scheme S2†) a $TPy^{3+}\cdot 3Cl^-$ molecule as a control compound. This control compound carries identical charges to $TPPC^{3+}$ but shows no binding with $Na_2C_2O_4$ in water (Fig. S44†). When we introduced 10% $TPy^{3+}\cdot 3Cl^-$ as a catalyst, we observed a slight rate acceleration for the oxidation of $HC_2O_4^-$ by $KMnO_4$, indicating that charge neutralization from electrostatic interactions is a critical factor for the rate acceleration. In comparison, we achieved an even faster rate of acceleration using only 1% of $TPPC^{3+}\cdot 3Cl^-$, suggesting that molecular recognition mediated by charge-assisted hydrogen bonding enhances the catalytic effect by more than tenfold. To further confirm that the rate acceleration of the reaction was directly attributable to the binding between $HC_2O_4^-$ and $TPPC^{3+}$, we performed (Fig. S63†) an additional control experiment by adding Na_2SO_4 (10 mM) as a competitive binding agent into a reaction mixture of $TPPC^{3+}\cdot 3Cl^-$ (0.01 mM), $KMnO_4$ (0.2 mM) and $H_2C_2O_4$ (1.0 mM). The consequent oxidation rate of $HC_2O_4^-$ decreased by 30% as a result of the competitive binding of SO_4^{2-} with $TPPC^{3+}$, serving as compelling evidence that the specific interaction between $HC_2O_4^-$ and $TPPC^{3+}$ is a pivotal factor in accelerating the reaction. To rule out the possibility of encapsulation of the anionic MnO_4^- by $TPPC^{3+}$, we examined a 1 : 1 mixture of $KMnO_4$ and $TPPC^{3+}\cdot 3Cl^-$ by ^1H NMR spectroscopy and observed (Fig. S43†) no change in chemical shift of $TPPC^{3+}\cdot 3Cl^-$, suggesting a lack of appreciable binding between MnO_4^- and $TPPC^{3+}$. HRMS analysis of a mixture of $KMnO_4$ and $TPPC^{3+}\cdot 3Cl^-$ confirmed (Fig. S11†) the absence of binding, as it only displayed peaks corresponding to the free $TPPC^{3+}$. Conversely, the HRMS spectra of a mixture containing $KMnO_4$, $H_2C_2O_4$, and $TPPC^{3+}\cdot 3Cl^-$ showed (Fig. S11†) a distinct peak at m/z 512.7495, pointing to the selective formation of the $HC_2O_4^-\subset TPPC^{3+}$ complex in the presence of the MnO_4^- anion.

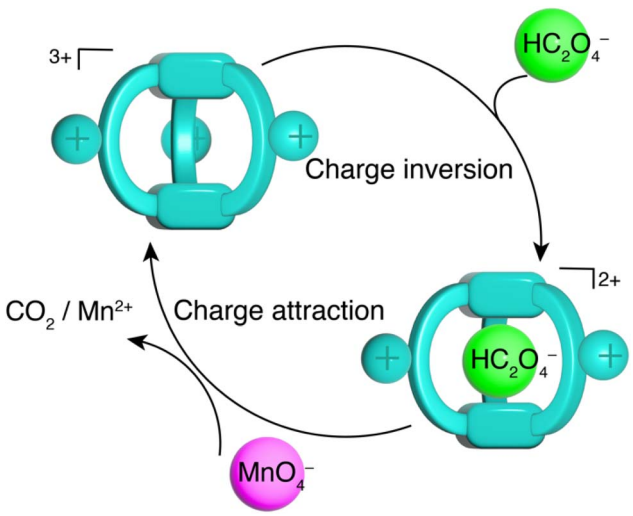

Fig. 8 Schematic illustration of the catalytic cycle of oxalate oxidation catalyzed by $TPPC^{3+}$.

Conclusions

In conclusion, a tangible outcome of this study is the development of the water-soluble amide cage, $TPPC^{3+}\cdot 3Cl^-$, which can be readily synthesized by a dynamic approach. This cage demonstrates strong affinities and excellent selectivities for hydrophilic anions in water. Notably, $TPPC^{3+}\cdot 3Cl^-$ exhibits remarkable binding affinities towards divalent anions such as $C_2O_4^{2-}$ and SO_4^{2-}, which play crucial roles in conditions like

kidney stone formation[98,99] and the management of radioactive nuclear waste,[100] respectively. These findings are poised to advance efforts in oxalate removal during hemodialysis and enhance sulfate separation processes in the treatment of nuclear waste. Moreover, this research introduces the encapsulation of an anionic substrate by a cationic cage as a new mechanism for catalysis in water. This molecular recognition approach effectively inverts the charges of the substrate and facilitates reactions by overcoming electrostatic repulsions, showcasing an innovative strategy for developing catalysts in water.

From a fundamental standpoint, our work broadened the scope of charge-assisted hydrogen bonding by illustrating its utility in an amide-type synthetic receptor, offering a general molecular design principle that applies to a wide range of amide receptors. This principle not only revalidates their hydrogen bonding capabilities but also opens avenues for the efficient molecular recognition of hydrophilic substrates in water. These findings will pave the way for the development of synthetic receptors for medical intervention,[101–105] anion sensing,[106–112] separation and sequestration,[10,100,113–115] and catalysis in biologically and environmentally relevant aqueous media.[116–120]

Data availability

The data supporting this article have been included as part of the ESI.†

Author contributions

C. X. and W. L. conceived and designed the project and wrote the manuscript. X. C., Q. T., D. L., C. Z. and W. L. performed the experiments and analyzed the results. L. W. solved the crystal structures.

Conflicts of interest

There are no conflicts to declare.

Acknowledgements

Financial support for this work was provided by the National Science Foundation (CHE-2337419) and the University of South Florida start-up funding. This research made use of the XRAY and CPAS Core facilities at the University of South Florida. The research was supported in part by the computational resources provided by the CIRCE research cluster facility at the University of South Florida.

Notes and references

1 G. A. Jeffrey and W. Saenger, *Hydrogen Bonding in Biological Structures*, Springer Berlin Heidelberg, Berlin, Heidelberg, 1991.
2 J. C.-H. Chen, B. L. Hanson, S. Z. Fisher, P. Langan and A. Y. Kovalevsky, *Proc. Natl. Acad. Sci. U.S.A.*, 2012, **109**, 15301–15306.
3 H. Luecke and F. A. Quiocho, *Nature*, 1990, **347**, 402–406.
4 J. W. Pflugrath and F. A. Quiocho, *Nature*, 1985, **314**, 257–260.
5 A. R. Fersht, J.-P. Shi, J. Knill-Jones, D. M. Lowe, A. J. Wilkinson, D. M. Blow, P. Brick, P. Carter, M. M. Y. Waye and G. Winter, *Nature*, 1985, **314**, 235–238.
6 J. Dong and A. P. Davis, *Angew. Chem., Int. Ed.*, 2021, **60**, 8035–8048.
7 M. J. Langton, C. J. Serpell and P. D. Beer, *Angew. Chem., Int. Ed.*, 2016, **55**, 1974–1987.
8 S. Kubik, *ChemistryOpen*, 2022, **11**, e202200028.
9 S. Kubik, *Chem. Soc. Rev.*, 2010, **39**, 3648.
10 J. Samanta, M. Tang, M. Zhang, R. P. Hughes, R. J. Staples and C. Ke, *J. Am. Chem. Soc.*, 2023, **145**, 21723–21728.
11 A. Metzger and E. V. Anslyn, *Angew. Chem., Int. Ed.*, 1998, **37**, 649–652.
12 J. Krämer, R. Kang, L. M. Grimm, L. De Cola, P. Picchetti and F. Biedermann, *Chem. Rev.*, 2022, **122**, 3459–3636.
13 C.-L. Deng, S. L. Murkli and L. D. Isaacs, *Chem. Soc. Rev.*, 2020, **49**, 7516–7532.
14 L. Escobar and P. Ballester, *Chem. Rev.*, 2021, **121**, 2445–2514.
15 I. V. Kolesnichenko and E. V. Anslyn, *Chem. Soc. Rev.*, 2017, **46**, 2385–2390.
16 G. T. Williams, C. J. E. Haynes, M. Fares, C. Caltagirone, J. R. Hiscock and P. A. Gale, *Chem. Soc. Rev.*, 2021, **50**, 2737–2763.
17 D. R. Carcanague, C. B. Knobler and F. Diederich, *J. Am. Chem. Soc.*, 1992, **114**, 1515–1517.
18 F. Diederich and D. R. Carcanague, *Helv. Chim. Acta*, 1994, **77**, 800–818.
19 E. M. Peck, W. Liu, G. T. Spence, S. K. Shaw, A. P. Davis, H. Destecroix and B. D. Smith, *J. Am. Chem. Soc.*, 2015, **137**, 8668–8671.
20 W. Liu, A. Johnson and B. D. Smith, *J. Am. Chem. Soc.*, 2018, **140**, 3361–3370.
21 A. P. Davis, *Chem. Soc. Rev.*, 2020, **49**, 2531–2545.
22 P. Stewart, C. M. Renney, T. J. Mooibroek, S. Ferheen and A. P. Davis, *Chem. Commun.*, 2018, **54**, 8649–8652.
23 P. Ríos, T. J. Mooibroek, T. S. Carter, C. Williams, M. R. Wilson, M. P. Crump and A. P. Davis, *Chem. Sci.*, 2017, **8**, 4056–4061.
24 P. Rios, T. S. Carter, T. J. Mooibroek, M. P. Crump, M. Lisbjerg, M. Pittelkow, N. T. Supekar, G. J. Boons and A. P. Davis, *Angew. Chem., Int. Ed.*, 2016, **55**, 3387–3392.
25 T. J. Mooibroek, J. M. Casas-Solvas, R. L. Harniman, C. M. Renney, T. S. Carter, M. P. Crump and A. P. Davis, *Nat. Chem.*, 2016, **8**, 69–74.
26 T. S. Carter, T. J. Mooibroek, P. F. N. Stewart, M. P. Crump, M. C. Galan and A. P. Davis, *Angew. Chem., Int. Ed.*, 2016, **55**, 9311–9315.
27 C. Ke, H. Destecroix, M. P. Crump and A. P. Davis, *Nat. Chem.*, 2012, **4**, 718–723.
28 D. H. Li and B. D. Smith, *Beilstein J. Org. Chem.*, 2019, **15**, 1086–1095.
29 W. Liu, C. F. A. Gómez-Durán and B. D. Smith, *J. Am. Chem. Soc.*, 2017, **139**, 6390–6395.

30 W. Liu, E. M. Peck, K. D. Hendzel and B. D. Smith, *Org. Lett.*, 2015, **17**, 5268–5271.
31 S. K. Shaw, W. Liu, S. P. Brennan, M. de Lourdes Betancourt-Mendiola and B. D. Smith, *Chem.–Eur. J.*, 2017, **23**, 12646–12654.
32 Y. F. Wang, H. Yao, L. P. Yang, M. Quan and W. Jiang, *Angew. Chem., Int. Ed.*, 2022, **61**, e202211853.
33 X. Wang, M. Quan, H. Yao, X. Y. Pang, H. Ke and W. Jiang, *Nat. Commun.*, 2022, **13**, 2291.
34 M. Li, Y. Dong, M. Quan and W. Jiang, *Angew. Chem., Int. Ed.*, 2022, **61**, e202208508.
35 X. Huang, X. Wang, M. Quan, H. Yao, H. Ke and W. Jiang, *Angew. Chem., Int. Ed.*, 2021, **60**, 1929–1935.
36 L. P. Yang, X. Wang, H. Yao and W. Jiang, *Acc. Chem. Res.*, 2020, **53**, 198–208.
37 H. Ke, L. P. Yang, M. Xie, Z. Chen, H. Yao and W. Jiang, *Nat. Chem.*, 2019, **11**, 470–477.
38 H. Yao, H. Ke, X. Zhang, S. J. Pan, M. S. Li, L. P. Yang, G. Schreckenbach and W. Jiang, *J. Am. Chem. Soc.*, 2018, **140**, 13466–13477.
39 L.-L. Wang, Z. Chen, W.-E. Liu, H. Ke, S.-H. Wang and W. Jiang, *J. Am. Chem. Soc.*, 2017, **139**, 8436–8439.
40 G. B. Huang, S. H. Wang, H. Ke, L. P. Yang and W. Jiang, *J. Am. Chem. Soc.*, 2016, **138**, 14550–14553.
41 S. Kubik, R. Kirchner, D. Nolting and J. Seidel, *J. Am. Chem. Soc.*, 2002, **124**, 12752–12760.
42 S. Otto and S. Kubik, *J. Am. Chem. Soc.*, 2003, **125**, 7804–7805.
43 Z. Rodriguez-Docampo, S. I. Pascu, S. Kubik and S. Otto, *J. Am. Chem. Soc.*, 2006, **128**, 11206–11210.
44 J. M. Llinares, D. Powell and K. Bowman-James, *Coord. Chem. Rev.*, 2003, **240**, 57–75.
45 E. García-España, P. Díaz, J. M. Llinares and A. Bianchi, *Coord. Chem. Rev.*, 2006, **250**, 2952–2986.
46 P. Blondeau, M. Segura, R. Pérez-Fernández and J. De Mendoza, *Chem. Soc. Rev.*, 2007, **36**, 198–210.
47 M. Berger and F. P. Schmidtchen, *Angew. Chem., Int. Ed.*, 1998, **37**, 2694–2696.
48 W. Peschke, P. Schiessl, F. P. Schmidtchen, P. Bissinger and A. Schier, *J. Org. Chem.*, 1995, **60**, 1039–1043.
49 A. Metzger, V. M. Lynch and E. V. Anslyn, *Angew. Chem., Int. Ed.*, 1997, **36**, 862–865.
50 M. D. Best, S. L. Tobey and E. V. Anslyn, *Coord. Chem. Rev.*, 2003, **240**, 3–15.
51 Q. Q. Wang, V. W. Day and K. Bowman-James, *Angew. Chem., Int. Ed.*, 2012, **51**, 2119–2123.
52 S. O. Kang, R. A. Begum and K. Bowman-James, *Angew. Chem., Int. Ed.*, 2006, **45**, 7882–7894.
53 K. Bowman-James, *Acc. Chem. Res.*, 2005, **38**, 671–678.
54 L. Chen, S. N. Berry, X. Wu, E. N. W. Howe and P. A. Gale, *Chem*, 2020, **6**, 61–141.
55 P. A. Gale, *Acc. Chem. Res.*, 2006, **39**, 465–475.
56 P. A. Gale and C. Caltagirone, *Chem. Soc. Rev.*, 2015, **44**, 4212–4227.
57 W. A. Harrell, M. L. Bergmeyer, P. Y. Zavalij and J. T. Davis, *Chem. Commun.*, 2010, **46**, 3950–3952.
58 J. T. Davis, P. A. Gale, O. A. Okunola, P. Prados, J. C. Iglesias-Sánchez, T. Torroba and R. Quesada, *Nat. Chem.*, 2009, **1**, 138–144.
59 A. P. Bisson, V. M. Lynch, M.-K. C. Monahan and E. V. Anslyn, *Angew. Chem., Int. Ed.*, 1997, **36**, 2340–2342.
60 L. Qin, S. J. N. Vervuurt, R. B. P. Elmes, S. N. Berry, N. Proschogo and K. A. Jolliffe, *Chem. Sci.*, 2020, **11**, 201–207.
61 V. E. Zwicker, K. K. Y. Yuen, D. G. Smith, J. Ho, L. Qin, P. Turner and K. A. Jolliffe, *Chem.–Eur. J.*, 2018, **24**, 1140–1150.
62 S. N. Berry, L. Qin, W. Lewis and K. A. Jolliffe, *Chem. Sci.*, 2020, **11**, 7015–7022.
63 Q. He, N. J. Williams, J. H. Oh, V. M. Lynch, S. K. Kim, B. A. Moyer and J. L. Sessler, *Angew. Chem., Int. Ed.*, 2018, **57**, 11924–11928.
64 Q. He, G. M. Peters, V. M. Lynch and J. L. Sessler, *Angew. Chem., Int. Ed.*, 2017, **56**, 13396–13400.
65 S. Peng, Q. He, G. I. Vargas-Zúñiga, L. Qin, I. Hwang, S. K. Kim, N. J. Heo, C. H. Lee, R. Dutta and J. L. Sessler, *Chem. Soc. Rev.*, 2020, **49**, 865–907.
66 Y. Liu, W. Zhao, C.-H. Chen and A. H. Flood, *Science*, 2019, **365**, 159–161.
67 H. Wang, S. Fang, G. Wu, Y. Lei, Q. Chen, H. Wang, Y. Wu, C. Lin, X. Hong, S. K. Kim, J. L. Sessler and H. Li, *J. Am. Chem. Soc.*, 2020, **142**, 20182–20190.
68 C. Zhai, C. Xu, Y. Cui, L. Wojtas and W. Liu, *Chem.–Eur. J.*, 2023, **29**, e202300524.
69 W. Liu, S. Bobbala, C. L. Stern, J. E. Hornick, Y. Liu, A. E. Enciso, E. A. Scott and J. Fraser Stoddart, *J. Am. Chem. Soc.*, 2020, **142**, 3165–3173.
70 W. Liu, C. Lin, J. A. Weber, C. L. Stern, R. M. Young, M. R. Wasielewski and J. F. Stoddart, *J. Am. Chem. Soc.*, 2020, **142**, 8938–8945.
71 W. Liu, Y. Tan, L. O. Jones, B. Song, Q. H. Guo, L. Zhang, Y. Qiu, Y. Feng, X. Y. Chen, G. C. Schatz and J. F. Stoddart, *J. Am. Chem. Soc.*, 2021, **143**, 15688–15700.
72 M. J. Langton, S. W. Robinson, I. Marques, V. Félix and P. D. Beer, *Nat. Chem.*, 2014, **6**, 1039–1043.
73 J. Lehr, T. Lang, O. A. Blackburn, T. A. Barendt, S. Faulkner, J. J. Davis and P. D. Beer, *Chem.–Eur. J.*, 2013, **19**, 15898–15906.
74 M. J. Langton and P. D. Beer, *Chem.–Eur. J.*, 2012, **18**, 14406–14412.
75 N. H. Evans, H. Rahman, A. V. Leontiev, N. D. Greenham, G. A. Orlowski, Q. Zeng, R. M. J. Jacobs, C. J. Serpell, N. L. Kilah, J. J. Davis and P. D. Beer, *Chem. Sci.*, 2012, **3**, 1080.
76 A. Brown and P. D. Beer, *Dalton Trans.*, 2012, **41**, 118–129.
77 N. H. Evans, C. J. Serpell, N. G. White and P. D. Beer, *Chem.–Eur. J.*, 2011, **17**, 12347–12354.
78 N. H. Evans and P. D. Beer, *Org. Biomol. Chem.*, 2011, **9**, 92–100.
79 S. R. Bayly, T. M. Gray, M. J. Chmielewski, J. J. Davis and P. D. Beer, *Chem. Commun.*, 2007, 2234.
80 G. Hennrich and E. V. Anslyn, *Chem.–Eur. J.*, 2002, **8**, 2218.

81 J. C. Lauer, A. S. Bhat, C. Barwig, N. Fritz, T. Kirschbaum, F. Rominger and M. Mastalerz, *Chem.–Eur. J.*, 2022, **28**, e202201527.
82 A. S. Bhat, S. M. Elbert, W. Zhang, F. Rominger, M. Dieckmann, R. R. Schröder and M. Mastalerz, *Angew. Chem., Int. Ed.*, 2019, **131**, 8911–8915.
83 $TPPC^{3+}$ showed a poor water solubility when associated with hydrophobic counter anions such as BF_4^- and PF_6^-, making it impractical to evaluate its anion binding properties in water.
84 R. S. Das, D. Maiti, S. Kar, T. Bera, A. Mukherjee, P. C. Saha, A. Mondal and S. Guha, *J. Am. Chem. Soc.*, 2023, **145**, 20451–20461.
85 A. Szumna and J. Jurczak, *Eur. J. Org Chem.*, 2001, 4031–4039.
86 M. J. Chmielewski and J. Jurczak, *Chem.–Eur. J.*, 2005, **11**, 6080–6094.
87 M. J. Chmielewski and J. Jurczak, *Chem.–Eur. J.*, 2006, **12**, 7652–7667.
88 A. Martinez-Cuezva, L. V. Rodrigues, C. Navarro, F. Carro-Guillen, L. Buriol, C. P. Frizzo, M. A. P. Martins, M. Alajarin and J. Berna, *J. Org. Chem.*, 2015, **80**, 10049–10059.
89 V. W. Liyana Gunawardana, C. Ward, H. Wang, J. H. Holbrook, E. R. Sekera, H. Cui, A. B. Hummon and J. D. Badjić, *Angew. Chem., Int. Ed.*, 2023, **62**, e202306722.
90 F. Biedermann, W. M. Nau and H. J. Schneider, *Angew. Chem., Int. Ed.*, 2014, **53**, 11158–11171.
91 A downfield shift of proton B was observed during the titration with Cl^-, while an upfield shift occurred when titrated with Br^- and I^-. The downfield shift of proton B indicates Cl^- binding to the partially filled cavity of the cage. The upfield shift with Br^- and I^- can be attributed to the displacement of Cl^- by these anions, which have lower charge densities and thus lead to a weaker ion-dipole interaction with proton B, resulting in its upfield shift.
92 C. M. Hindson, Z. M. Smith, N. W. Barnett, G. R. Hanson, K. F. Lim and P. S. Francis, *J. Phys. Chem. A*, 2013, **117**, 3918–3924.
93 M. A. Kelland, *J. Chem. Educ.*, 2011, **88**, 276–278.
94 K. A. Kovács, P. Gróf, L. Burai and M. Riedel, *J. Phys. Chem. A*, 2004, **108**, 11026–11031.
95 V. Pimienta, D. Lavabre, G. Levy and J. C. Micheau, *J. Phys. Chem.*, 1995, **99**, 14365–14371.
96 H. F. Launer, *J. Am. Chem. Soc.*, 1932, **54**, 2597–2610.
97 ^1H NMR titration experiment between $H_2C_2O_4$ and $TPPC^{3+}\cdot 3Cl^-$ revealed (Fig. S41 and S42†) a binding constant of $3.8 \times 10^5\ M^{-1}$ in water.
98 T. Ermer, C. Kopp, J. R. Asplin, I. Granja, M. A. Perazella, M. Reichel, T. D. Nolin, K.-U. Eckardt, P. S. Aronson, F. O. Finkelstein and F. Knauf, *Kidney International Reports*, 2017, **2**, 1050–1058.
99 C. F. M. Franssen, *Nephrol., Dial., Transplant.*, 2005, **20**, 1916–1921.
100 C. J. Fowler, T. J. Haverlock, B. A. Moyer, J. A. Shriver, D. E. Gross, M. Marquez, J. L. Sessler, M. A. Hossain and K. Bowman-James, *J. Am. Chem. Soc.*, 2008, **130**, 14386–14387.
101 P. A. Gale, J. T. Davis and R. Quesada, *Chem. Soc. Rev.*, 2017, **46**, 2497–2519.
102 E. S. Williams, H. Gneid, S. R. Marshall, M. J. González, J. A. Mandelbaum and N. Busschaert, *Org. Biomol. Chem.*, 2022, **20**, 5958–5966.
103 S. R. Herschede, R. Salam, H. Gneid and N. Busschaert, *Supramol. Chem.*, 2022, **34**, 26–33.
104 R. Salam, S. M. Chowdhury, S. R. Marshall, H. Gneid and N. Busschaert, *Chem. Commun.*, 2021, **57**, 13122–13125.
105 R. Cao, R. B. Rossdeutcher, Y. Zhong, Y. Shen, D. P. Miller, T. A. Sobiech, X. Wu, L. S. Buitrago, K. Ramcharan, M. I. Gutay, M. F. Figueira, P. Luthra, E. Zurek, T. Szyperski, B. Button, Z. Shao and B. Gong, *Nat. Chem.*, 2023, **15**, 1559–1568.
106 R. Hein, P. D. Beer and J. J. Davis, *Chem. Rev.*, 2020, **120**, 1888–1935.
107 N. H. Evans and P. D. Beer, *Angew. Chem., Int. Ed.*, 2014, **53**, 11716–11754.
108 K. M. Bak, S. C. Patrick, X. Li, P. D. Beer and J. J. Davis, *Angew. Chem., Int. Ed.*, 2023, **62**, e202300867.
109 R. Hein, A. Docker, J. J. Davis and P. D. Beer, *J. Am. Chem. Soc.*, 2022, **144**, 8827–8836.
110 R. Hein and P. D. Beer, *Chem. Sci.*, 2022, **13**, 7098–7125.
111 S. C. Patrick, R. Hein, P. D. Beer and J. J. Davis, *J. Am. Chem. Soc.*, 2021, **143**, 19199–19206.
112 P. D. Beer and P. A. Gale, *Angew. Chem., Int. Ed.*, 2001, **40**, 486–516.
113 C. R. Benson, L. Kacenauskaite, K. L. VanDenburgh, W. Zhao, B. Qiao, T. Sadhukhan, M. Pink, J. Chen, S. Borgi, C. H. Chen, B. J. Davis, Y. C. Simon, K. Raghavachari, B. W. Laursen and A. H. Flood, *Chem*, 2020, **6**, 1978–1997.
114 A. Aydogan, D. J. Coady, S. K. Kim, A. Akar, C. W. Bielawski, M. Marquez and J. L. Sessler, *Angew. Chem., Int. Ed.*, 2008, **47**, 9648–9652.
115 S. K. Kim, J. Lee, N. J. Williams, V. M. Lynch, B. P. Hay, B. A. Moyer and J. L. Sessler, *J. Am. Chem. Soc.*, 2014, **136**, 15079–15085.
116 J. M. Ovian, P. Vojáčková and E. N. Jacobsen, *Nature*, 2023, **616**, 84–89.
117 Q. Li, S. M. Levi, C. C. Wagen, A. E. Wendlandt and E. N. Jacobsen, *Nature*, 2022, **608**, 74–79.
118 S. M. Banik, A. Levina, A. M. Hyde and E. N. Jacobsen, *Science*, 2017, **358**, 761–764.
119 M. S. Taylor and E. N. Jacobsen, *Angew. Chem., Int. Ed.*, 2006, **45**, 1520–1543.
120 T. Du, B. Shen, J. Dai, M. Zhang, X. Chen, P. Yu and Y. Liu, *J. Am. Chem. Soc.*, 2023, **145**, 27788–27799.